International Journal of Climatology

International Journal of Climatology RMetS

RESEARCH ARTICLE

Dynamic and Thermodynamic Contributions to Future Extreme-Rainfall Intensification: A Case Study for Belgium

Jozefien Schoofs[1,2] | Kobe Vandelanotte[1,3] | Hans Van de Vyver[1] | Line Van Der Sichel[3] | Matthias Vandersteene[3] | Fien Serras[2] | Nicole P. M. van Lipzig[2] | Bert Van Schaeybroeck[1,4]

[1]Department of Meteorological and Climatological Research, Royal Meteorological Institute, Brussels, Belgium | [2]Department of Earth and Environmental Sciences, KU Leuven, Leuven, Belgium | [3]Department of Physics and Astronomy, Ghent University, Ghent, Belgium | [4]Department of Geography, Ghent University, Ghent, Belgium

Correspondence: Jozefien Schoofs (jozefien.schoofs@kuleuven.be)

Received: 5 February 2025 | **Revised:** 30 October 2025 | **Accepted:** 6 November 2025

Keywords: circulation patterns | climate change | CMIP6 | dynamical changes | extreme precipitation | Lamb weather types | model selection

ABSTRACT

Extreme precipitation is projected to become more frequent and more intense due to climate change and associated thermodynamical effects, but the local response of atmospheric circulation under future climate scenarios remains uncertain due mainly to dynamical differences. In this study, we outline a methodology for a regional assessment of future extreme precipitation based on the Lamb Weather Type classification and to evaluate future changes in weather patterns. Whilst anticyclonic days occur most frequently over Belgium, extreme rainfall is mostly associated with days of cyclonic, westerly and south-westerly weather patterns. GCMs from CMIP6 are first selected based on their reliability in representing local atmospheric circulation patterns during days with extreme rainfall. It was found that for our case study over Belgium, the future (end-of-the-century SSP3-7.0) changes in intensity and likelihood of rainfall extremes can be primarily attributed to thermodynamic factors, with minimal contribution from changes in atmospheric dynamics. Both intensity and probability of extreme rainfall increase for all seasons. Whilst extreme-rainfall probabilities mostly increase in fall and winter, the associated intensity increases are largest in fall. Additionally, the weather patterns that are historically associated with extreme rainfall, disproportionately contribute to these changes, especially to thermodynamic changes. More specifically, robust changes arise from an increased extreme-rainfall occurrence probability in the case of cyclonic, south-westerly and westerly circulation types.

1 | Introduction

Extreme rainfall events have become more frequent in Western and Central Europe and are very likely to increase further as climate change continues (IPCC 2021). Its intensity is projected to increase throughout the world in the future warming climate, the rate of which is dependent on the scenario considered (Hansen et al. 2024). As extreme precipitation events can lead to flooding, landslides and other natural disasters, they will significantly impact different aspects of the environment, society and economy (Gutiérrez et al. 2021; IPCC 2022). In recent years, several catastrophic events took place over Europe, where warming rates are higher than the global one. In mid-July 2021, Germany, Belgium, Luxembourg and the Netherlands were hit by 3 days of excessive rainfall leading to more than 200 fatalities and enormous infrastructural damage (Tradowsky et al. 2023). In September 2024, the storm Boris caused record-breaking rainfall and devastating floods over a wide area in Central and Eastern Europe. Athanase et al. (2024) identified an additional 9% of rainfall and an 18% larger area affected by the storm due to human-induced warming. A month later, in October 2024, another record-breaking downpour led to flash floods over Sevilla (Spain), ensuing again over 200 fatalities (World Weather Attribution 2024). In a rapid analysis, the World Weather

Attribution working group estimated that this rainfall was approximately 12% heavier and twice as likely compared to a pre-industrial climate. Flood risks are generally exacerbated by a high degree of urbanisation, as is present in Belgium, associated with an enhanced degree of surface runoff and reduced groundwater recharge and evapotranspiration (Mees et al. 2015). In Belgium, for instance, urban expansion was shown to lead to a 20% increase in runoff between 1976 and 2000, a trend which is further intensifying (Poelmans et al. 2010).

It is well established that atmospheric circulation plays a determining role in driving precipitation variability over Europe (Brisson et al. 2011; Pattison and Lane 2012; Planchon et al. 2009; Richardson et al. 2018; Whitford et al. 2024). Several methods have been proposed to categorise these atmospheric circulation types (CTs) (Huth et al. 2008) and several works have investigated the historical CT connection with climatic variables such as rainfall (Brisson et al. 2011; Cotterill et al. 2023), extreme precipitation (Tramblay et al. 2013), heatwaves (Serras et al. 2024), floods (Pattison and Lane 2012; Richardson, Neal, et al. 2020), droughts (Richardson, Fowler, et al. 2020), sea level rise (Perks et al. 2023) and the influence of circulation on weather extremes in general (Faranda et al. 2023; Pfahl 2014).

CTs also allow one to better understand regional climate changes. Whilst, as expressed by the Clausius–Clapeyron equation, warmer air can hold more moisture and therefore extreme rainfall is expected to be more intense (Neelin et al. 2022), changes in the CTs occurrence frequencies may oppose or strengthen this trend regionally. Hansen et al. (2024) focus on the relation between CTs and extreme precipitation and find it is stable under climate change over Scandinavia. Herrera-Lormendez et al. (2023) examined shifts in future CTs under a high-emission scenario and their impact on average summer precipitation and droughts. Finally, similar to the study of Cattiaux et al. (2013) for cold extremes, Otero et al. (2018) use CTs to disentangle future changes in temperature into changes related to CT-frequency changes (i.e., dynamical changes) and temperature changes within each CT (i.e., thermodynamical changes). As far as we are aware, however, the role of the dynamical and thermodynamical contributions to changes in extreme-rainfall frequency and intensity and their seasonal dependence over Central Europe has not been investigated. As far as we are aware, however, the role of weather types in changes in extreme rainfall frequency and intensity and their seasonal dependence over Central Europe has not been investigated.

In line with observations, Global Circulation Models (GCMs) consistently show the large-scale intensification of precipitation extremes in a warming climate (Giorgi et al. 2019). However, projecting these changes at regional and local scales remains challenging (Hansen et al. 2024) especially their interpretation in terms of physical mechanisms (Neelin et al. 2022; O'Gorman 2015). Additionally, despite their consistent improvements of the latest generation of CMIP6 GCMs (Eyring et al. 2016) with respect to CMIP5, GCMs suffer from difficulties in capturing regional circulation patterns (Brands 2022; Vautard et al. 2023). In order to account for this, some works select models based on their reliability in capturing the historical climatological features of CT (e.g., McSweeney et al. 2015; Serras et al. 2024).

In this study, we focus on the CTs specifically associated with extreme-rainfall days to enhance regional projections. The objective here is to better understand future changes in extreme precipitation over Belgium. Therefore we develop a methodology for regional assessment of future extreme precipitation, focusing on the influence of atmospheric circulation patterns, and to evaluate how changes in atmospheric circulations and thermodynamic factors will impact the intensity and likelihood of extreme rainfall events. We therefore (i) identify the relationship between atmospheric circulation patterns and daily precipitation extremes, (ii) evaluate the GCM performance based on their reliability to reproduce atmospheric patterns linked to extreme precipitation, and (iii) decompose the intensity and likelihood changes of extreme rainfall into dynamic and thermodynamic contributions through a case study over Belgium. To assess the relationship between CTs and extreme precipitation, a commonly used circulation-classification methodology, the Lamb Weather Type (LWT) classification (Brisson et al. 2011; Otero et al. 2018; Serras et al. 2024), is used.

2 | Materials and Methods

2.1 | Study Area

Belgium is situated in Western Europe (see Figure 1) and features a temperate maritime climate, strongly influenced by the North Atlantic Ocean and characterised by relatively mild temperatures with little variation throughout the year (Brisson et al. 2011). Precipitation patterns over Belgium are heavily affected by large-scale atmospheric circulation, including the North Atlantic Oscillation, especially in wintertime. Fronts from the west, which are associated with cyclonic events, are responsible for most of the precipitation. Brisson et al. (2011) also showed that winter days are often wetter than days in other seasons but have a low average rainfall intensity over Belgium. In summer, in contrast, the rainfall intensity is higher. Therefore, in winter, long periods of persistent rainfall occur more often, whereas, in summer, extreme precipitation in shorter periods is more likely to be catastrophic. Large-scale frontal systems typically drive winter extreme precipitation events, whilst summer extremes are often driven by localised convective processes (Richardson, Neal, et al. 2020).

Belgium is highly populated, urbanised and industrialised, making it particularly vulnerable to extreme weather events such as heat waves, thunderstorms and different types of flooding (De Troch et al. 2020; Termonia et al. 2018). Additionally, Belgium's varied orography has a notable effect on both average precipitation and extreme weather events (Journée et al. 2015; Van de Vyver 2012; Vanden Broucke et al. 2019; Wyard et al. 2017) with annual average rainfall that varies from 600 mm/year near the coast to 1400 mm/year in the orographic regions (RMI Atlas 2024).

2.2 | Data

Observed precipitation data were used to investigate the relationship between the weather types and past extreme precipitation. Daily rain-gauge data were used for the period 1951–2023 at the

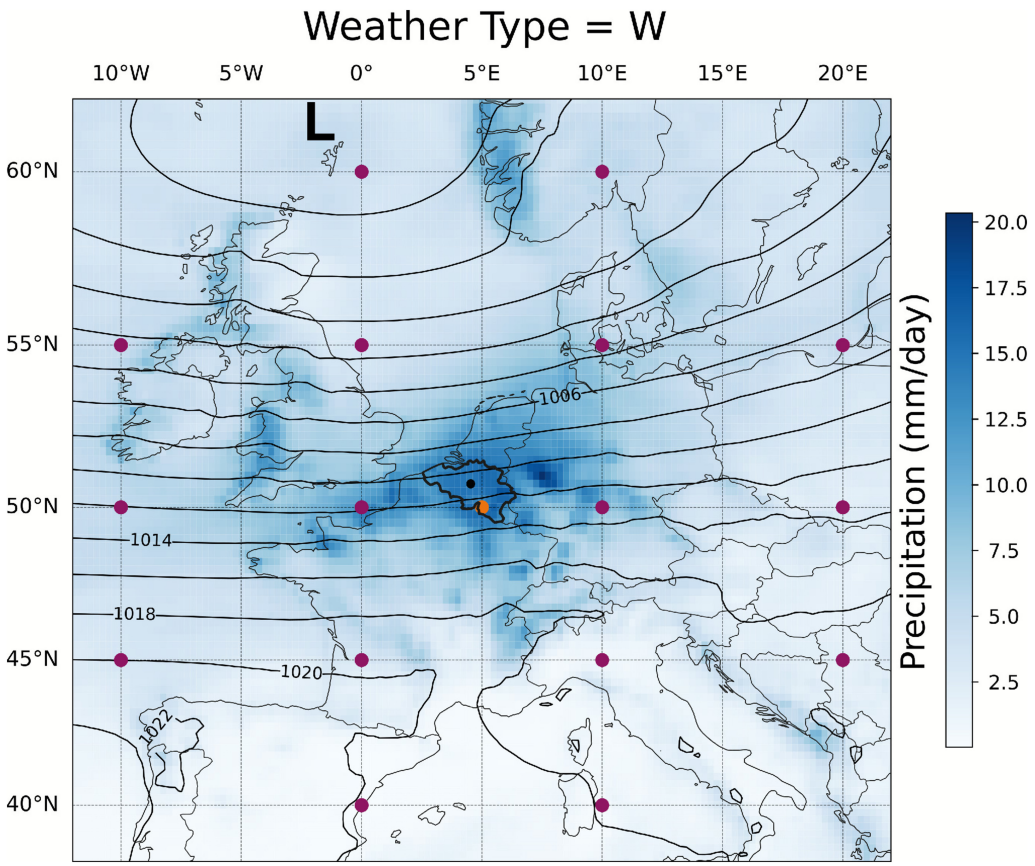

FIGURE 1 | Map of Western Europe with Belgium indicated with bold borders in the centre. Mean sea level pressure from ERA5 at the 16 red-dotted points are used to determine the weather pattern over Belgium. Contours indicate the average pressure for the pattern with western flow (W) whilst the blue shading indicate the average ERA5 rainfall during extreme-rainfall days with western flow for the period 1979–2019. The Uccle observation station (50.7975° N, 4.3592° E) is indicated with a black point. [Colour figure can be viewed at wileyonlinelibrary.com]

station of Uccle (Belgium), managed by the Royal Meteorological Institute of Belgium.

To determine the weather types, we use ERA5, an atmospheric global reanalysis that embodies a detailed record of the global atmosphere, land surface and ocean waves from 1940 onwards (Hersbach et al. 2020). ERA5 is the fifth and latest generation of reanalysis produced by the European Centre for Medium-Range Weather Forecasts (ECMWF). Daily mean sea level pressure (MSLP) at a resolution of 0.25°×0.25° over Europe from 1951 to 2023 was used to establish the LWTs. For the model evaluation, the period 1985–2014 is used as this coincides with the last 30 years of the CMIP6 historical simulations.

To evaluate potential changes in extreme precipitation due to climate change, a set of state-of-the-art coupled global climate models (GCMs) from the CMIP6 project is used. CMIP is a project of the World Climate Research Programme (WCRP)'s Working Group of Coupled Modelling (Eyring et al. 2016). An ensemble of 24 models with one member per model is considered since different ensemble members of GCMs are expected to feature similar atmospheric circulation patterns (Belleflamme et al. 2013), hence giving equal weight to each model. Following Serras et al. (2024), different model families are used to obtain the widest possible range of model diversity. An overview of the selected CMIP6 models is given in Table S1. We already excluded the CMIP6 models that were the least effective in reproducing the LWTs over Belgium during the summer-time period, as this is the most important period for extreme rainfall (Serras et al. 2024).

For each model, we utilise the historical or reference period 1985–2014, and the future period 2069–2098 of the Shared Socioeconomic Pathways SSP3-7.0. This pathway represents a medium-to-high forcing scenario (i.e., a radiative forcing level of 7 W/m^2 in 2100) under a regional-rivalry scenario (i.e., SSP3) (Guo et al. 2022) and it is chosen because of its expected higher signal-to-noise ratio. A 30-year period is chosen, in line with the guidelines of the WMO.

2.3 | Definition of Extreme Rainfall

Under current climate conditions, a day with extreme precipitation over Belgium is defined in VMM (2023) as a day with 20 mm/day or more of local rainfall at Uccle. In order to generalise this definition towards a modelling context, we define extreme rainfall using a well-established quantile-based method (Vautard et al. 2016) to fix a high threshold. Thereby, we identify extreme-rainfall days for CMIP6 model output based on the quantile of daily precipitation that corresponds to this 20 mm/day in the observations, that is the 98.87th quantile, within the historical period and in the gridpoint closest to the observation station. A day with extreme precipitation in the CMIP6 model

(both historical and future) is then defined as a day with rainfall that exceeds this model-dependent threshold. By using this 'quantile-mapping' method, consistency in identifying days with extreme rainfall across both observed and modelled data is ensured. Finally, the extreme-rainfall intensity is the rainfall amount above the threshold on a day of extreme rainfall. Its average is therefore not an average over all days but only over those with extreme rainfall. Note that we also test the sensitivity of our results with respect to a threshold corresponding to the 95th quantile of daily rainfall (11.32 mm) instead of the 98.87th quantile (20 mm).

2.4 | Lamb Weather Types

In this study, we use the objective CT classification methodology introduced by Lamb and Office (1972), and later adjusted by Jenkinson and Collison (1977), known as the LWT classification or the 'Jenksinson–Collison Weather Type' classification. For a detailed explanation of the original LWT classification algorithm we refer to Serras et al. (2024). The circulation pattern at a given day is characterised by the positioning of high and low-pressure centres which control the orientation of the geostrophic airflow (Otero et al. 2018). The LWT classification uses the MSLP on a 16-point grid with a footprint of 30° longitudes by 20° latitudes surrounding the centre point at 50° N and 5° E (in Belgium) for which the LWT is defined. This central point is relatively close to the Uccle observation station (50.7975° N, 4.3592° E). From the MSLP of the 16 grid points, six indices are calculated that characterise the direction and vorticity of the geostrophic flow. That is, the westerly and southerly flow components describe the area's primary zonal and meridional airflow, whilst total shear vorticity indicates atmospheric rotation. The classification of the LWT depends on the balance between the overall flow and the total vorticity.

We use eight directional weather types (N, NE, E, SE, S, SW, W, NW), two non-directional vorticity weather types (cyclonic C and anticyclonic A) and an unclassified weather type (low flow, LF). These are obtained by merging the original 27 LWTs following the approach of Demuzere et al. (2009). Table 1 tabulates the synoptic situation over Belgium for each weather type. In this study, a distinction is made between wet and dry LWTs for Belgium (Table 1). Days with more than 1 mm are classified as wet. A weather type, on the other hand, is considered wet (dry) if its occurrence probability is higher (lower) on a rainy day than on an average day (Figure S2). Note that the same classification of LWTs into wet and dry types is found if one uses days with extreme rainfall instead of wet days (see Figure S2). For illustrative purposes, we show in Figure 1 the average ERA5 MSLP and extreme-rainfall intensity during days of western flow (see Figure S1 for the other LWTs).

Finally, note that not all CMIP6 GCMs have days of extreme precipitation for all weather types. For example, seven models did not project extreme precipitation for weather type SE, whereas for the cyclonic weather type C, all models did. Additionally, not all models project extreme precipitation to be present with weather types A and SE in the future period considered. Only 5 out of 19 models have days of extreme rainfall during weather type A, and two for SE. We tabulate all weather types without days of extreme rainfall per GCM in Table S1.

TABLE 1 | Overview of the two vorticity, eight directional and low flow (LF) Lamb Weather Types (LWTs), their acronym and description, as well as their precipitation classification for Belgium.

Weather type	Description	Wet/dry
Vorticity types		
Anticyclonic (A)	Anticyclones centred over, near or extending over Belgium	Dry
Cyclonic (C)	Low pressure centred stagnating over, or frequently passing across Belgium	Wet
Directional types		
Easterly (E)	Anticyclones north of Belgium, between Scandinavia and Iceland, and cyclones south of Belgium, in the Azores-Spain-Biscay region	Dry
Northerly (N)	High pressure to the west and north-west of Belgium, and low pressure to the east and north-east of Belgium	Wet
North-easterly (NE)	Anticyclone over Scandinavia and cyclones south of Belgium	Dry
North-westerly (NW)	Anticyclone of the Azores displaced north to north-east towards Belgium, and depressions located north-east to Belgium	Wet
Southerly (S)	High pressure covering central and northern Europe, North Atlantic depressions west of Belgium	Dry
South-easterly (SE)	Anticyclones over central or eastern Europe	Dry
South-westerly (SW)	Low pressure systems over the North Atlantic	Wet
Westerly (W)	High pressure to the south and low pressure to the north of Belgium	Wet
Low flow (LF)	Weak pressure gradients covering Europe	Dry

Note: The wet and dry days are defined based on the occurrence probabilities shown in Figure S2. Finally, Figure S1 shows the average surface pressure fields and average rainfall per LWT over the domain used.

2.5 | Circulation-Based Model Evaluation and Selection

We evaluate the reproducibility of LWT probability during days of extreme rainfall for CMIP6 models as compared to ERA5 over the reference period (1985–2014). Based on this assessment, the worst-performing models are eliminated from further analysis.

In order to quantify the dissimilarity between the LWT probability density functions of ERA5 (O) and the CMIP6 models (M), we use both the original Perkins Skill Score (PSS) (Perkins et al. 2007; Serras et al. 2024) and a squared Perkins Skill Score (sPSS):

$$\mathrm{PSS} = 1 - \frac{1}{2}\sum_i \left|Q^M_{i,\mathrm{ext}} - Q^O_{i,\mathrm{ext}}\right| \quad \text{and} \quad \mathrm{sPSS} = 1 - \frac{1}{2}\sum_i \left(Q^M_{i,\mathrm{ext}} - Q^O_{i,\mathrm{ext}}\right)^2 \tag{1}$$

where i is the LWT, and $Q^M_{i,\mathrm{ext}}$ and $Q^O_{i,\mathrm{ext}}$ the probability of LWT i during days of extreme rainfall of the model and reference distribution, respectively. If a model perfectly reproduces the reference probabilities, PSS and sPSS are equal to 1 whilst a value of 0 is obtained in case of a complete mismatch. In this work, we opt for the use of sPSS as it penalises large occurrence-probability errors which are especially present when models misrepresent the most important weather types (during days of extreme rainfall). Based on their sPSS, models are ranked, and those with an sPSS value below the mean minus one standard deviation, are excluded from further analysis, similar to the approach in Serras et al. (2024).

2.6 | Decomposition Into Dynamic and Thermodynamic Contributions

The goal here is to understand the future increase in extreme rainfall frequency and intensity over Belgium in terms of changes in 'dynamics' and 'thermodynamics'.

Assume $P_{\mathrm{ext}}(x_t)$ is the rainfall exceedance probability above a fixed high threshold x_t (here 20 mm/day, 98.87th quantile) and for which we are interested in its change $\Delta P_{\mathrm{ext}}(x_t) = P^{\mathrm{f}}_{\mathrm{ext}}(x_t) - P^{\mathrm{h}}_{\mathrm{ext}}(x_t)$ between the future (f) and historical (h) period. This change can be written as a sum over LWTs i, with a proof given in Section S1 (Barry and Perry 1973; Otero et al. 2018; Souverijns et al. 2016; Vautard et al. 2016):

$$\Delta P_{\mathrm{ext}}(x_t) = \sum_i \underbrace{P^{\mathrm{f}}_{i,\mathrm{ext}}(x_t)\Delta Q_{i,\mathrm{clim}}}_{\text{Dyn.}} + \underbrace{Q^{\mathrm{h}}_{i,\mathrm{clim}}\Delta P_{i,\mathrm{ext}}(x_t)}_{\text{Thermodyn.}} \tag{2}$$

where $P_{i,\mathrm{ext}}(x_t)$ is the rainfall exceedance probability for days of LWT i, $Q_{i,\mathrm{clim}}$ is the probability of LWT i over all days and Δ indicates the difference between the future and historical value. The first part of the equation represents the dynamic change induced by changes in the occurrence probability of the weather types. The second part, henceforth denoted as the thermodynamic contribution, quantifies the changes of the rainfall exceedance probability given a certain LWT. Apart from changes in the large-scale thermodynamics, this term may also encompass local or mesoscale feedbacks, or (despite its naming) even dynamic changes outside of the European domain that affect moisture advection towards Europe (Souverijns et al. 2016).

The rainfall intensity $I(x_t)$ was defined as the average excess rainfall above a fixed high threshold x_t on days of extreme rainfall (i.e., with rainfall above x_t). Similar to Equation (2), the intensity change under climate change can be written as (see also Section S1):

$$\Delta I(x_t) = \sum_i \underbrace{I^{\mathrm{f}}_i(x_t)\Delta Q_{i,\mathrm{ext}}}_{\text{Dyn.}} + \underbrace{Q^{\mathrm{h}}_{i,\mathrm{ext}}\Delta I_i(x_t)}_{\text{Thermodyn.}} \tag{3}$$

where $I_i(x_t)$ is the average rainfall intensity during extreme-rainfall days of LWT i and $Q_{i,\mathrm{ext}}$ is the probability of LWT i for extreme-rainfall days. The dynamic and thermodynamic changes in rainfall intensity are therefore caused by LWT frequency changes and within-LWT intensity changes, respectively, *but both only during days of extreme rainfall*. The amount of extreme rainfall days may, however, differ between the historical and future periods but these differences are expressed by the extreme-rainfall probability changes $\Delta P_{\mathrm{ext}}(x_t)$ given in Equation (2).

3 | Results

3.1 | Observed Weather-Type Distribution and Link With Extreme Rainfall

Prior to analysing future changes in extreme precipitation characteristics, we examine the current-day probability of the LWTs, for all days (Q_{clim}, i.e., climatological probability), for wet days and for days with extreme precipitation (Q_{ext}), based on the station observations at Uccle (Belgium). The weather-type probabilities in the historical period (1951–2023) are depicted in Figure 2 and Figure S2. There are clear LWT probability differences amongst average days (grey bars), wet days (purple in Figure S2), and days with extreme precipitation (blue bars).

Whilst anticyclonic (A) days occur most often over Belgium (i.e., 22.1%), they rarely coincide with days of extreme rainfall (see Figure 2). Likewise, the probability of LWTs E, NE, S and SE is lower during days of extreme rainfall than their climatological probability, which is already low. Therefore, the above-mentioned dry LWTs (A, E, NE, S and SE) coincide very rarely with days of extreme rainfall. During days of extreme rainfall, the westerly (W), cyclonic (C) and south-westerly (SW) types occur most frequently, more specifically 25.3%, 20.8% and 19.9% (see Figure 2a). For W, this is 1.9 times higher than its climatological probability. Apart from W and SW, cyclonic (C) days are especially connected to extreme rainfall, since they feature an occurrence probability of 20.8%, whilst C has a low climatological probability of 6.7%. Furthermore, for northern (N) flow, the occurrence probability during days of extreme rainfall exceeds the climatological probability whilst both

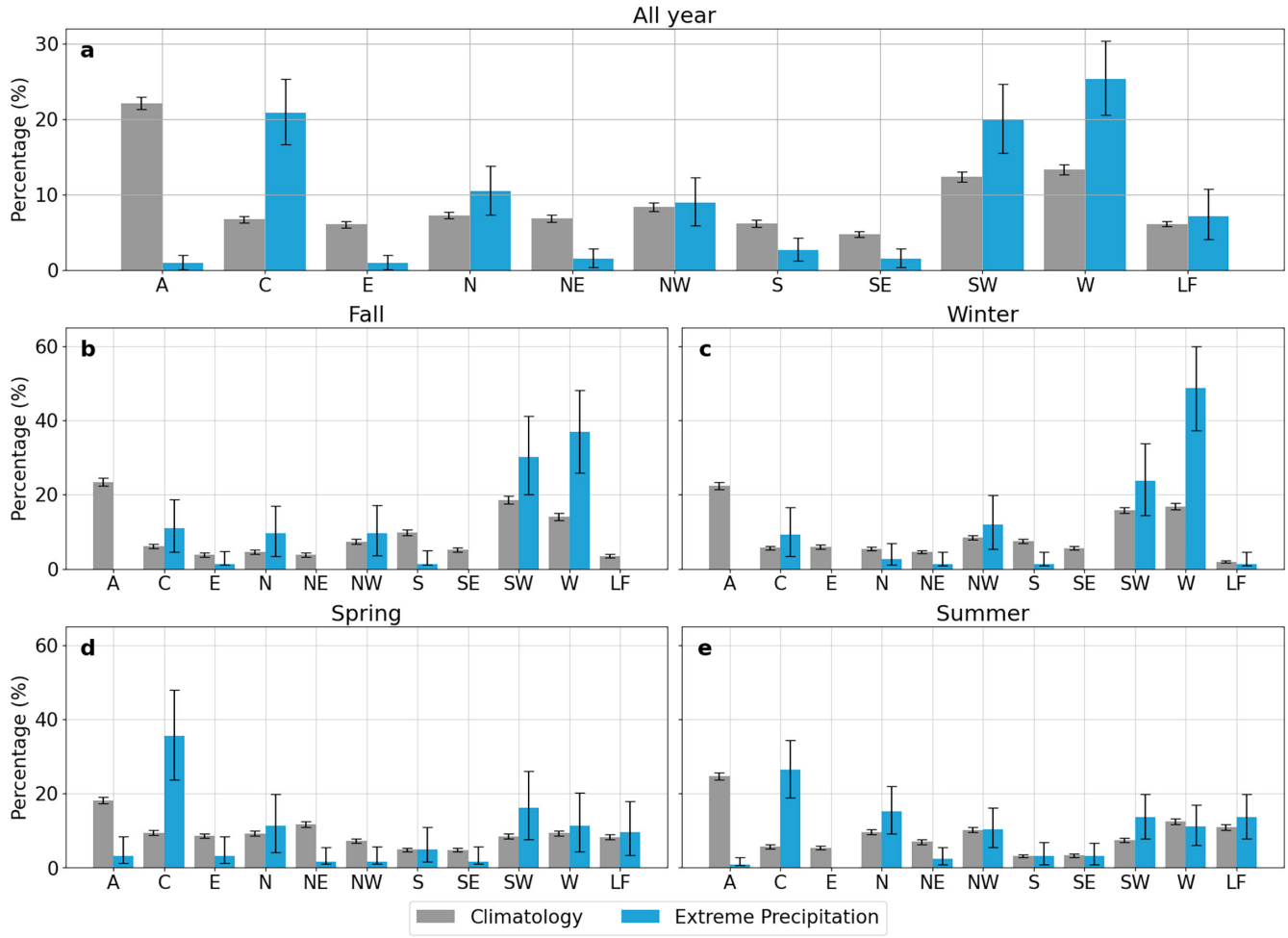

FIGURE 2 | Barplots representing the weather-type occurrence probability using ERA5 MSLP data and station precipitation at the grid box closest to Uccle (Belgium) during the period 1951–2023. The grey bars indicate the probability of weather types for all days Q_{clim} (i.e., the climatology) whilst the blue bars indicate the probability during days of extreme precipitation Q_{ext} (which, in total, constitute about 1.13% of all days). The top panel (a) presents the data for the whole year whilst the four seasons are presented in the panels (b)–(e). Error bars were created using 10^5 bootstrap samples. The weather types are described in Table 1. [Colour figure can be viewed at wileyonlinelibrary.com]

probabilities more or less coincide for NW. Lastly, the probability of the LF LWT is similar between the two categories (5.7% and 4.0%).

Within the considered period (1951–2023), 3051 days of extreme rainfall were found, out of which 40% (1250 cases) occurred during summer. Fall, winter and spring, on the other hand, each account for 20% of extreme-rainfall days. Figure 2b–e shows the variations in the LWT occurrence probability per season. Qualitatively, the extreme-rainfall probability in fall strongly resembles those in winter and those in spring resemble those in summer. Climatologically, anticyclonic days are the most prevalent in every season, reaching more than 20% in each season (except in spring with 18.2%). During days of extreme rainfall, on the other hand, LWT W is most prevalent in fall and winter (37.0% and 48.7%, respectively), and C in spring and summer (35.5% and 26.4%).

The cyclonic weather type was substantially less associated with extreme precipitation in fall and winter as compared to spring and summer. In spring and summer C occurred most frequently during days of extreme rainfall, that is 26.4% in summer which is 4.6 times its climatological occurrence frequency.

The 95% confidence intervals (CIs) of the LWT probabilities in Figure 2 were calculated using 10^5 resamples, obtained with a bootstrap procedure with replacement. As expected, due to the reduced sample sizes for days with extreme rainfall, the associated error bars are generally larger than those for the climatological probability.

3.2 | Model Evaluation and Selection

In order to subselect models from the CMIP6 ensemble, we assess how the GCMs reproduce the circulation patterns over Belgium during days with extreme rainfall for the reference period (1985–2014) based on the sPSS (Serras et al. 2024). We evaluate the sPSS for various variables, including the climatological LWT probability (Q_{clim}) and the LWT probability during extreme-rainfall days (Q_{ext}). The analysis revealed a low correlation (0.29, see Figure S6) between the sPSS of the climatological LWT probability (Q_{clim}) and that of the LWT probability during

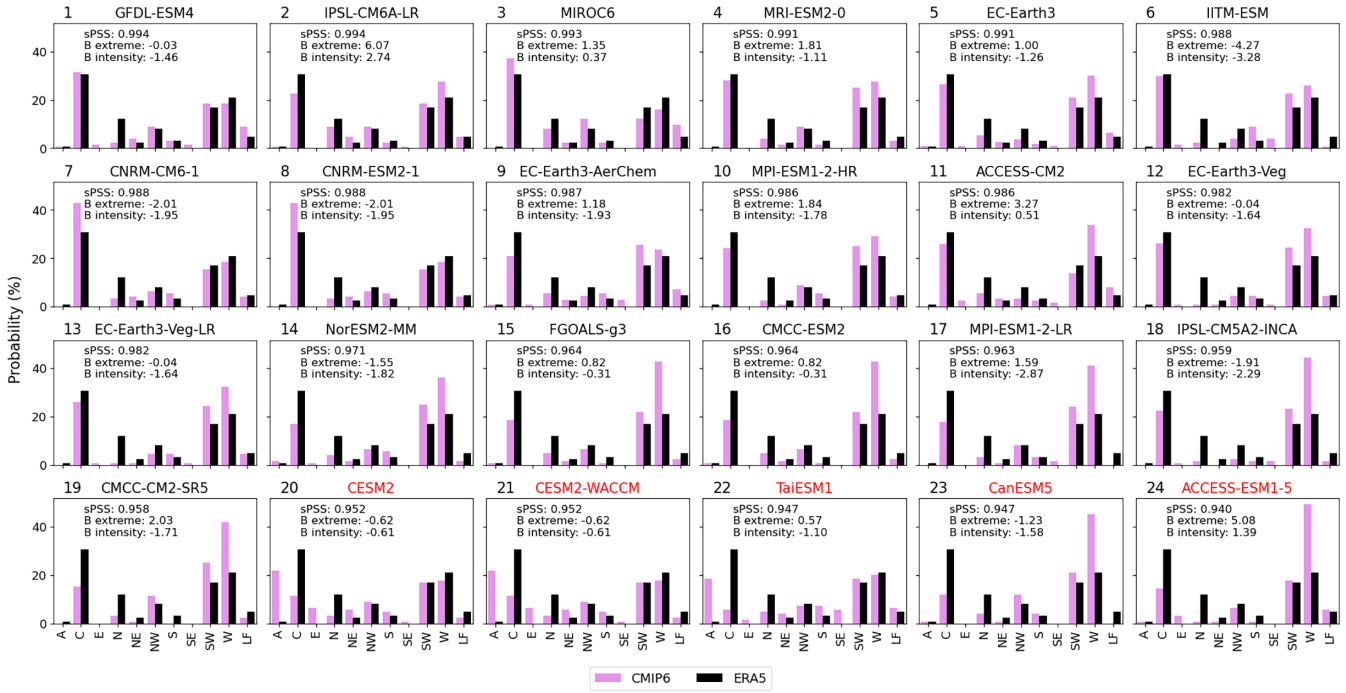

FIGURE 3 | Barplots representing the weather-type occurrence probability during days of extreme precipitation in Uccle (Belgium) for the different CMIP6 models (purple bars), compared against the reference data (ERA5, black bars) for the historical period 1985–2014. The squared Perkins Skill Score (sPSS) and its rank are indicated per model. Additionally, 'B extreme' indicates the bias in the 98.87th quantile of daily precipitation (in mm) and 'B intensity' corresponds to the bias in the intensity beyond that threshold. Models with a sPSS score below 0.956 are removed from the dataset for further analysis and are indicated in orange. [Colour figure can be viewed at wileyonlinelibrary.com]

extreme-rainfall days (Q_{ext}). These results suggest that a model's ability to accurately represent the climatological weather types is not necessarily an indicator of its skill in representing the LWT distribution during extreme precipitation events.

Figure 3 shows the LWT occurrence probabilities per model during days of extreme rainfall. Overall, there is a reasonable agreement between the model and the ERA5 probabilities and the agreement is quantified using the sPSS (see Equation 1) which is indicated in each panel. The sPSS values range from 0.940 to 0.994 amongst the models, and the panels in Figure 3 are ranked from high to low sPSS. The models therefore vary significantly in their accuracy of reproducing LWT probability during the reference period. As aforementioned, the sPSS threshold for model elimination is defined as the mean minus the standard deviation of the PSS which here is 0.956. Five out of 24 models (i.e., CESM2, CESM2-WACCM, TaiESM1, CanESM5 and ACCESS-ESM1-5) fall (slightly) below this performance threshold and are excluded from further analysis and are indicated in orange in Figure 3. Three out of five lowest-performing models (i.e., CESM2-WACCM, CESM2, TaiESM1) originate from one model family, that is CAM. Note, however, that the CanESM5 model was previously identified as the best model to represent the average circulation probability distribution over Belgium (Serras et al. 2024).

TaiESM1, CESM2 and CESM2-WACCM strongly overestimate the occurrence frequency of the anticyclonic (A) weather type and underestimate the cyclonic (C) weather type during extreme precipitation. For CanESM5 and ACCESS-ESM1-5, the largest discrepancies are found for weather type W. Caution has to be taken that even the best-performing models are far from perfect. Here, the best-performing model GFDL-ESM4 has an sPSS score of only 0.994. Additionally, MPI-ESM1-2-HR has an sPSS score of 0.986 and rank 10. This model strongly overestimates LWTs SW and W, and underestimates LWTs C and N during extreme precipitation. To conclude, the following climate-change analysis for Belgium will use only the 19 selected GCMs as the eliminated models may compromise reliability and accuracy.

A comparison of the model selection based on sPSS (Figure 3) against that of PSS (Figure S3) confirms that large occurrence-probability errors, and in particular those for the most important weather types, are more strongly penalised. For instance CMCC-CM2-SR5 and ACCESS-ESM1-5 strongly underestimate the occurrence probability of C leading to a sharp decline in their rank based on sPSS with respect to their rank based on PSS. Yet, four out of five models are common amongst the sets of discarded models for PSS and sPSS. More specifically, IPSL-CM5A2-INCA is discarded for PSS and ACCESS-ESM1-5 based on sPSS. This leads us to conclude that the selection method is relatively insensitive to variations in the scoring approach.

Finally, we find that the GCM model rank was uncorrelated with the model bias in extreme rainfall as shown in Figure S12. Therefore, a potential model selection based on the model grid-point representation of extreme rainfall would yield a strongly different set of models than the one based on circulation representation during extreme-rainfall days as presented here. For instance, the model featuring the largest bias in extreme-rainfall threshold occurs for IPSL-CM6A-LR which is the second-best model in terms of sPSS score.

3.3 | Total Intensity and Likelihood Changes

Figure 4a shows the relative change in extreme-rainfall intensity (green boxplot) in the future period (2069–2098) compared to the reference period (1985–2014) for the SSP3-7.0 scenario. The median of the relative change is 15.01% (green bar), which corresponds to 0.56 mm/day in absolute change (see Figure S7). There is a big spread amongst the different models in the magnitude of change with 3 out of 19 models showing an intensity decrease; more specifically, −10.82% for NorESM2-MM, −2.67% for IPSL-CM5A2-INCA and −1.67% for IPSL-CM6A-LR, corresponding to reductions in intensity of 0.49 mm/day, 0.11 mm/day and 0.14 mm/day, respectively. The CNRM-CM6-1 model features the highest relative change value of 51.39%, an intensity increase of 2.28 mm/day.

As seen in Equation (3), the total intensity changes can be split into the contributions of the dynamics and thermodynamics, indicated with orange and blue boxes in Figure 4a, respectively. By far the strongest contribution is attributable to the thermodynamics, that is changes in the properties of weather types. The median thermodynamic change is 13.39% (0.69 mm/day) and this is a robust result as 89% of the models agree on the sign of change. The dynamic contribution on the other hand, cannot be considered significantly different from zero.

Figure 4b shows the total relative change (green) in occurrence probability of days with extreme rainfall and their decomposition into the dynamic change (orange) and thermodynamic changes (blue). The median relative likelihood change is 42.74% and all models feature positive changes, ranging from 16.94% for CNRM-ESM2-1 to 75.0% for EC-Earth3-Veg. In other words, whilst, by definition, the historical occurrence probability of days with extreme precipitation is equal to 1.13% for all models (see Section 2.3), by the end-of-the-century following SSP3-7.0, this likelihood is expected to increase to 1.6% on average.

As was the case for the intensity changes, the thermodynamic contribution is responsible for the largest positive changes in extreme-rainfall probability whilst the (absolute) dynamic changes are comparatively very small. However, as opposed to the dynamic contribution of the intensity changes (orange bar in Figure 4a), the dynamic contribution to the extreme-rainfall likelihood changes is small but robustly negative with 84% of the models agreeing on the sign (orange bar in Figure 4b). More specifically, the dynamic contribution to the likelihood of days with extreme precipitation would decline by 5.43%. The thermodynamic probability changes, on the other hand, are positive for all models, indicating a likelihood increase of days with extreme precipitation with 49.79% (median value) due to within-type changes. As a result, thermodynamic changes have the largest contribution to the total changes in the likelihood.

3.4 | Weather-Type Contributions Under Climate Change

3.4.1 | Intensity Changes Per LWT

The contributions per LWT to the total relative changes in extreme-rainfall intensity are plotted in Figure 5a in the green boxplots (the absolute changes are shown in Figure S9a and the underlying terms from Equation (3) are shown in Figure S10a–e). All weather types, except for LF, show an increase in median intensity.

The largest total extreme-rainfall intensity increase is found for SW (5.62% or 0.246 mm/day) for which approximately 84% of the models show a positive change in intensity. The projected intensity increases for weather types C and W are comparatively large, but show larger uncertainties. The smallest increases are associated with the weather types N and S, followed by A, E and NW. The changes for NE, SE and LF, however, have a near-zero median. For Belgium, the weather types A, E, NE and SE are associated with dry weather. To elaborate, in the observed historical period (1985–2014), these weather types corresponded to 89.3% (A), 93.7% (E) and 91.5% (SE) of dry days, as well as (almost) no extreme precipitation in the reference and future period.

The dynamic and thermodynamic contributions to the intensity changes per weather type are also shown in Figure 5a. The wet weather types (i.e., C, N, W, SW, see Figure 2) occur most often for days with extreme precipitation, and show the

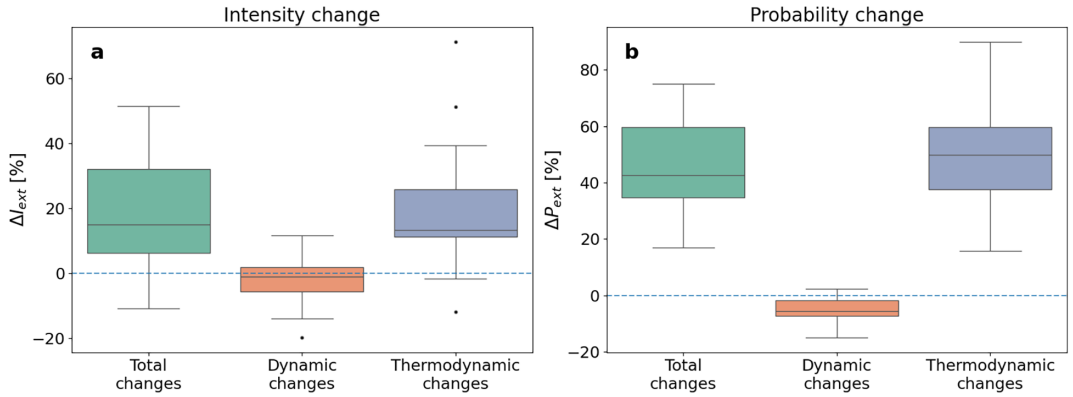

FIGURE 4 | Relative change in intensity (a) and occurrence probability (b) for days with extreme precipitation for 2069–2098 (following SSP3-7.0) with respect to 1985–2014, according to the 19 selected CMIP6 models. The green boxplot represents the total change in intensity, whilst the orange and blue indicate the dynamic and thermodynamic contributions, respectively. The median, interquartile range and outliers of these changes over the CMIP6 models are represented by the solid black line, the box and black dots, respectively. [Colour figure can be viewed at wileyonlinelibrary.com]

largest range of dynamic and thermodynamic changes. Their dynamic contributions decrease the extreme-rainfall intensity by about −2.18% (C) and −1.74% (W). These changes are relatively reliable for C as 74% of the models project negative changes but less reliable for W (only 63% of model agreement). Given that the (median) thermodynamic changes exceed the dynamic changes, the total changes for C and W are positive. The south-westerly (SW) weather type has the largest total changes with positive dynamic and thermodynamic changes, featuring the highest thermodynamic changes of all LWTs (i.e., 2.27% or 0.12 mm/day), and a thermodynamic contribution of 0.14% (0.01 mm/day).

3.4.2 | Probability Changes Per LWT

The total changes in the extreme-rainfall occurrence probability changes per weather type are presented as green boxplots in Figure 5b (the absolute changes are shown in Figure S9b and the underlying terms from Equation (2) are shown in Figure S10f–j). The wet weather types C, SW and W show positive increases (of magnitude 8.9%, 14.5% and 10.5%, respectively) that are much larger than those of the other LWTs. Additionally, the percentage of models indicating positive likelihood changes is also high, that is 95% (C), 89% (SW) and 100% (W). The remaining weather types feature much smaller, yet mostly statistically insignificant, total changes.

The most prevalent weather types C, SW and W during days of extreme precipitation (see Figure 2) also show the largest thermodynamic changes (orange bars in Figure S9b), that is 11.7% (C), 15.9% (SW) and 11.3% (W), with a strong agreement in sign amongst models, that is 95% for C and SW, and 100% for W, corresponding to 18 (19) out of 19 models (i.e., not for CNRM-CM6-1 for C, and GFDL-ESM4 for SW). Dynamic changes of C and W, on the other hand, indicate a decrease in occurrence probability due to weather-type frequency changes, with a reduction of 4.4% and 0.4%, respectively. For SW, the change is slightly positive, with 73% of models indicating a positive change.

Dry weather types like A, E and SE, which historically are not related to extreme precipitation, show minimal dynamic changes, with small total changes primarily due to thermodynamics. Other dry types such as NE, S and LF bring slightly more extreme precipitation, but changes in frequency and within-type intensity are minor. The wet types, NW and N, show a wider range of changes, indicating greater model disagreement on the magnitude of change.

3.5 | Changes Per Season

Figure 6a shows the total, dynamic and thermodynamic changes for the extreme-rainfall intensity per season. During spring and fall, the total changes (green bars) are higher than in summer and winter with large dynamical changes in spring and summer. The intensity changes are the smallest in winter. The seasonal contrasts are even more conspicuous for the changes in extreme-rainfall occurrence probability (Figure 6b) for which the biggest total changes occur now in fall and winter. The dynamic changes are small as compared to the thermodynamic changes for all seasons and are significantly negative for spring and summer and significantly positive in winter.

Note that the uncertainties associated with the total changes per season indicated in Figure 6 are frequently smaller than those of the thermodynamic contributions. This is indicative of compensation effects or negative correlations between the thermodynamic and dynamic contributions. These could arise due to future changes in the weather-type distribution that are decoupled from changes in extreme rainfall and may suggest that impact-tailored weather-type clustering methods (e.g., Serras et al. 2024) may be more suited to investigate these seasonal changes in extreme rainfall.

The contributions per weather type to the changes per season are shown in Figure 7 where, again, the largest contributions arise from a few wet weather types (C, SW, W). Whilst most changes are statistically insignificant for the intensity changes (Figure 7a–d),

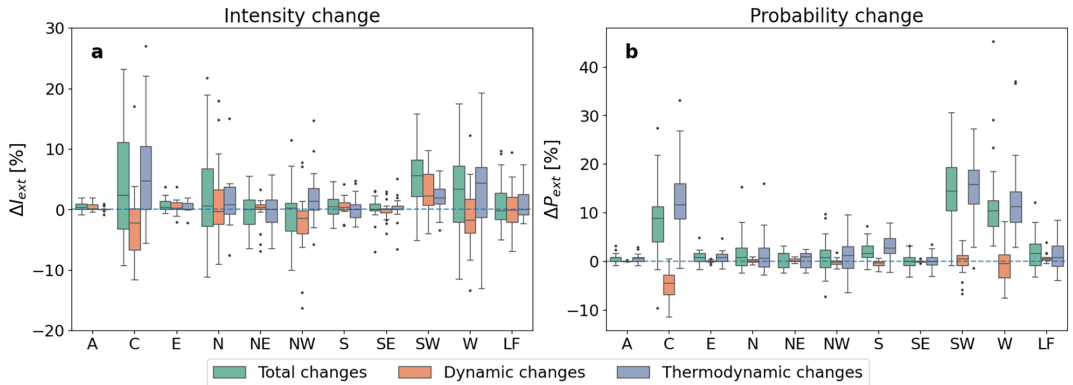

FIGURE 5 | Relative change in intensity (a) and occurrence probability (b) of extreme-precipitation days per weather type for 2069–2098 (following SSP3-7.0) with respect to 1985–2014, with bar plots showing the distributions of 19 CMIP6 models. The green boxplot represents the total relative change in intensity, and the orange and blue indicate the dynamic and thermodynamic contributions, respectively. The median, interquartile range and outliers of these changes over the CMIP6 models are represented by the solid black line, the box and black dots, respectively. Note that the *relative* changes are relative with respect to the total intensity and total probability (not those per LWT). Furthermore, the *y*-axis of (a) is clipped between −20% and 30% masking the following outliers: For C, CNRM-CM6-1 has a dynamic contribution of 42.9%, and a thermodynamic contribution of 55.8%. [Colour figure can be viewed at wileyonlinelibrary.com]

some are for the frequency changes (Figure 7e–h). More specifically, the large increases in extreme-rainfall probability in fall and winter are associated with both dynamic and thermodynamic increases for SW and W. The cyclonic weather type (C) also contributes significantly positive total changes in fall and winter but also in spring and summer. However, these positive total changes consistently involve large positive thermodynamic and small but significantly negative dynamic contributions due to reductions in the cyclonic occurrence probability (Figure 7e,g,h).

4 | Discussion

4.1 | Analysis of Observed Weather-Type Probability

We identified wet LWTs for Belgium including cyclonic (C), and the directional types westerly (W) and south-westerly (SW). In accordance with Brisson et al. (2011) in which the analysis was performed using wet-day likelihood, the following weather types were defined as wet: northerly (N) and north-westerly (NW). These weather types are more prevalent during extreme-rainfall days compared to their climatological likelihoods in the considered reference period (1951–2023). This finding broadly supports the work of other studies in this area (e.g., Hellström 2005 for Scandinavia and Herrera-Lormendez et al. 2023 for Western Europe). Richardson, Neal, et al. (2020) remark that the CTs associated with the highest probabilities of extreme precipitation are region dependent. Weather types W, SW and NW are often associated with precipitation as they transport warm maritime air from the North Atlantic (Brisson et al. 2011; Herrera-Lormendez et al. 2023; Trigo and DaCamara 2000). The western LWT (W) is most prevalent in fall and winter during days of extreme precipitation, whereas it is not very common in spring and summer. In fall and winter, the North Sea and North Atlantic Ocean are relatively warmer than land due to the large heat capacity of water. As a result, maritime air cools down over land

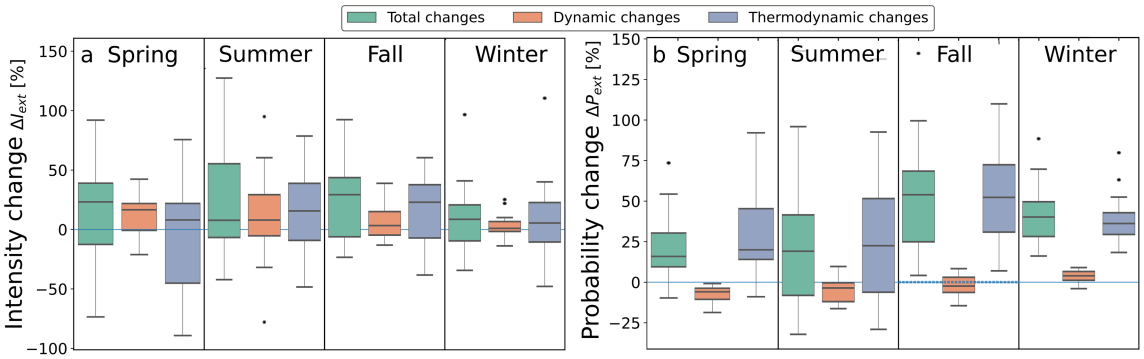

FIGURE 6 | Relative change in intensity (a) and occurrence probability (b) per season for days with extreme precipitation for 2069–2098 (following SSP3-7.0) with respect to 1985–2014, according to the 19 selected CMIP6 models in Uccle, Belgium. The green boxplot represents the total change in intensity, whilst the orange and blue indicate the dynamic and thermodynamic contributions, respectively. The median, interquartile range and outliers of these changes over the CMIP6 models are represented by the solid black line, the box and black dots, respectively. [Colour figure can be viewed at wileyonlinelibrary.com]

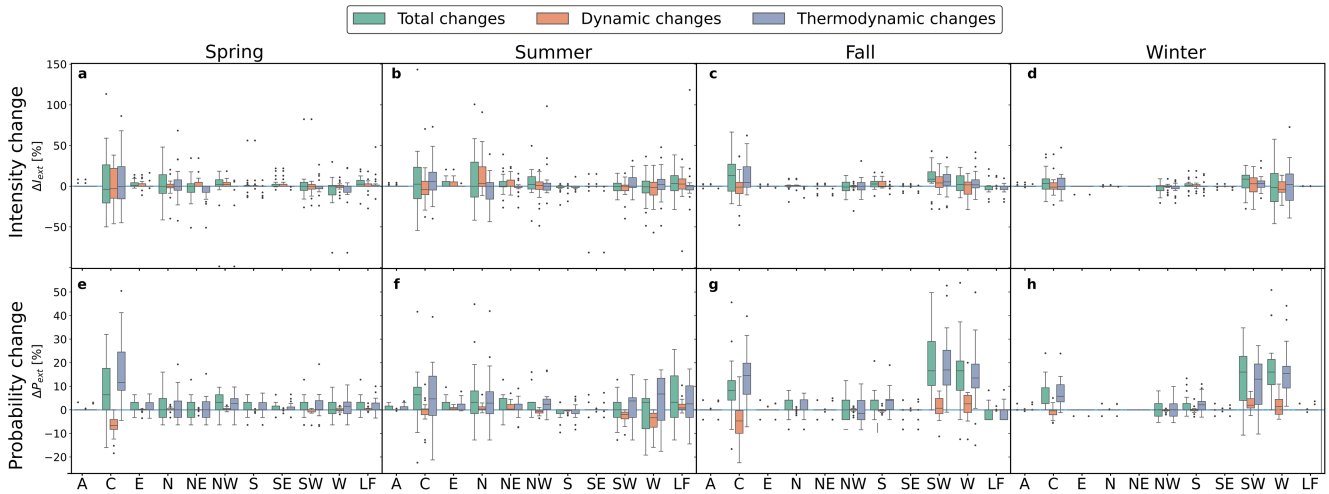

FIGURE 7 | Relative seasonal change in intensity (a–d) and occurrence probability (e–h) of extreme-precipitation days per weather type for 2069–2098 (following SSP3-7.0) with respect to 1985–2014 for Uccle (Belgium), with bar plots showing the distributions of 19 CMIP6 models. The green boxplot represents the total relative change in intensity, and the orange and blue indicate the dynamic and thermodynamic contributions, respectively. The median, interquartile range and outliers of these changes over the CMIP6 models are represented by the solid black line, the box and black dots, respectively. Note that the *relative* changes are relative w.r.t. to the total intensity and total probability (not those per LWT). [Colour figure can be viewed at wileyonlinelibrary.com]

and a high degree of condensation may lead to more (extreme) precipitation than in spring and summer for W. Furthermore, blocking anticyclonic events in regions to the northeast, northwest and sometimes to the south of Belgium generally increase the likelihood of extreme rainfall, as described by Lenggenhager and Martius (2019). These can correspond to the weather types NW, N and W.

Furthermore, the work in Herrera-Lormendez et al. (2023) describes synoptic atmospheric patterns within the summer climatology. Over Europe, anticyclonic circulation (A) was found to be the most common, occurring on 20% of days, supporting our findings of a 22% year-round likelihood over Belgium. In addition to A, weather types E, NE, SE and S which are connected to continental geostrophic flow, indicate dry conditions in Western Europe according to Herrera-Lormendez et al. (2023) and in our results. This work also indicates that the low-flow conditions have no dominating impact on precipitation across most of Europe, due to a lack of moisture advection, which is in line with our findings.

Prior studies (e.g., Schiemann and Frei 2010) have noted that CTs more effectively capture mesoscale precipitation variability in mid-latitudes during winter as compared to summer. This might lead to a lower likelihood of wet LWTs for days with extreme rainfall during summer (Brisson et al. 2011), consistent with our results. In contrast, during winter extreme rainfall, the smallest variability within LWTs is found, with a dominance of weather type W.

4.2 | Model Evaluation and Selection

The study by Brands (2022) indicates that models in CMIP6 generally outperform their CMIP5 counterparts regarding the recurring regional atmospheric circulation patterns in global models. In the study by Li et al. (2021), CMIP6 models are evaluated for their ability to capture daily rainfall extremes. They found reasonable accuracy in comparison to reanalysis data (Li et al. 2021). However, these models still have some limitations. Shepherd (2014) identifies that uncertainties in atmospheric pattern projections stem mainly from natural internal variability, systematic model errors and external influences such as volcanic and solar variability. The difficulty in accurately modeling small-scale processes affecting broader circulation patterns further contributes to these projection uncertainties (Shepherd 2014).

Brands (2022) found a strong correlation between model performance in producing regional atmospheric circulation patterns in global models and horizontal resolution, with higher-resolution models generating better results. Moreover, they found different levels of performance accuracy across different regions. Brands (2022) also suggests that the CMCC and NorESM2 model results are indicative of the CESM2 model results (for which the data was not available) as all derive from the NCAR model. This was, however, not confirmed by our analysis as, unlike the CMCC and NorESM2 models, CESM2 and CESM2-WACCM were discarded from the analysis and with distinct LWT biases during days of extreme rainfall (see Figure 3). This may be due to differences in convective parametrization schemes that are important for extreme rainfall. Additionally, contrary to our results for days of extreme rainfall, Brands (2022) found TaiESM1 to perform well over Europe.

Our work extends the methodology of Serras et al. (2024) to extreme rainfall. The threshold metric used is the sPSS which evaluates the distance of the LWT probability distribution during extreme-rainfall days between the model and the reference ERA5 (Figure S2). Apart from the climatological LWT probability (Q_{clim}) and the LWT probability during days of extreme rainfall (Q_{ext}), we also considered the sPSS metric for the conditional probability of extreme rainfall given the occurrence of LWT i: ($Q_{cond} \propto Q_{ext}/Q_{clim}$). The correlation between the sPSS of the LWT probability fraction (Q_{cond}) and the one of Q_{ext} is quite high (0.84, see Figure S11), whilst the one between Q_{cond} and Q_{clim} is low (0.13, see Figure S11). This indicates the dominant influence of the sPSS during extreme-precipitation days on the sPSS of Q_{cond}. Therefore, we consider it justified to use the sPSS score for days with extreme precipitation (Q_{ext}) to distinguish models.

The GCM selection methodology in Serras et al. (2024) limits the risk of choosing models with inadequate representation of the synoptic-scale dynamics. Their model assessment focused on the climatology for June, July and August, and there were substantial differences in model rankings between their and our analysis. This highlights the importance of evaluating models to determine their suitability for the intended application and is in line with the low correlation between the sPSS of the climatological LWT distribution and the one during days of extreme rainfall.

Figure S4 shows the equivalent of Figure 3 but using the 95th quantile of daily rainfall instead of the 98.87th quantile. Despite the slight changes in model ranks, the set of selected GCMs remains unchanged, regardless of whether the 95th or the 98.87th quantile is used. When performing the model selection based on PSS instead of sPSS for the 95th quantile (see Figure S5) four out of the five previously discarded models remain. This confirms the robustness of our selection methodology with respect to changes in the threshold.

4.3 | Intensity and Likelihood Changes and Their Decomposition

A strong agreement in the sign of change for extreme-precipitation intensity has been reported in the literature at a global scale (IPCC 2021), with increases in intensity largely attributable to anthropogenic influence (Tabari et al. 2020; Tradowsky et al. 2023). CMIP6 climate projections, for example, foresee an increase in the number of very heavy rain days globally, with higher significance under higher SSP scenarios (Feng et al. 2023). Whilst extreme precipitation will become more frequent, light-to-moderate precipitation may decline due to the drying and stabilising effects of intense rainfall (Li et al. 2021; Thackeray et al. 2022). Our research aligns with these findings, identifying a relative intensity and probability increase of days with extreme rainfall under a future SSP3-7.0 scenario in Belgium at 15.01% and 42.74%, respectively. Note that future increases in the intensity and likelihood of extreme

rainfall might even be larger than current model projections, since CMIP6 models may underestimate the historical scaling of precipitation extremes with global mean temperature (Kotz et al. 2024). Furthermore, Cotterill et al. (2023) reported that, although mean autumn precipitation decreased over Great Britain, the probability of extreme daily rainfall events increased by 71%–103% under an RCP8.5 scenario. This range is comparable to what we found for Belgium under an SSP3-7.0 scenario.

Our results also align quite well with the results of Pope et al. (2022) based on the CMIP5 ensemble and a single-model ensemble of the UK Met Office Global Coupled Model for the British Isles. They find an increase in winter weather types associated with cyclonic and westerly conditions. We also find an increase in W and SW occurrence but also a small decrease in cyclonic type (see green bars in Figure S10i). For summer, Pope et al. (2022) find an increase in dry settled weather types with a corresponding reduction in the wet weather types. Similarly, Figure S10i indicates a strong increase in the dry or stable weather types (A, LF, NE and E) at the expense of more wet weather types (NW) but also a dry weather type (S, SW, W).

The present study aimed to determine the dynamical and thermodynamical contributions to the changes in future extreme precipitation over Belgium. Consistent with previous work (e.g., Herrera-Lormendez et al. 2023; Kuettel et al. 2011; Otero et al. 2018; Tabari et al. 2020), thermodynamics is found to be the primary contributor to future changes, driven by the intensification of the hydrological cycle under global warming (IPCC 2021). Rising temperatures enhance atmospheric water-holding capacity by approximately 7% per °C, as described by the Clausius–Clapeyron relation (IPCC 2021), leading to increased evaporation and moisture availability, and consequently raising the potential for extreme precipitation events when the air mass cools and condenses. This trend is particularly evident in mid-to-high latitudes, including Belgium, and results in a relatively uniform global fractional increase in extreme-precipitation intensity (Pfahl et al. 2017). Dynamic factors, on the other hand, can offset the aforementioned effects in some areas (e.g., Mediterranean) but do not appear for Belgium, aligning with for example Tabari et al. (2020).

Our results demonstrate an increase in intensity and likelihood of extreme rainfall days under CTs C, SW and W (Figure 2). The increase in likelihood is in line with for instance Zappa et al. (2013), who found an increase in the number of cyclones associated with extreme precipitation over the North Atlantic and Europe, whilst cyclonic occurrences were found to decrease. In line with our results (for W, NW and SW), Herrera-Lormendez et al. (2023) found a projected likelihood decrease for the most important wet LWTs (C, W, NW, and SW) for summer over Europe, leading to the projected drying trend in Western-European summers following SSP5-8.5 (Herrera-Lormendez et al. 2023).

We used Equations (2) and (3) to decompose into a thermodynamic and a dynamic component and extended it to the case of extreme-precipitation intensity and probability. Our 'thermodynamic' changes are defined as those changes that are not due to changes in weather-type frequencies and may therefore not fully align with those in other works, especially those that are more process based. This is, however, a commonly used simplification. In fact, all the processes that are responsible for a change in precipitation within a specific LWT are allocated to the thermodynamic term, whilst several non-thermodynamic processes are likely to occur. During dry LWTs, mesoscale features must be present on extreme-precipitation days, that facilitate the initiation of convective processes, or at least processes capable of sustaining high rainfall rates over a prolonged period (Whitford et al. 2024). It also needs to be acknowledged that dynamic and thermodynamic processes interact across different scales, and linking extreme precipitation events to a single atmospheric process is an oversimplification (Prein et al. 2023). For instance, rainfall extremes are influenced by the temperatures at which they occur (O'Gorman and Schneider 2009). Furthermore, seasonal differences further complicate the picture, as convective processes dominate in summer, whilst synoptic systems and large-scale ocean-to-land moisture transport play a more significant role in winter (Brogli et al. 2019).

The dynamical term takes into account only the changes in the probability of large-scale LWTs. A poleward expansion of the tropical Hadley circulation in fall and winter (Grise and Davis 2020) is often mentioned to be responsible for changes in LWT. As a response, a poleward shift of westerly-like weather types will take place (Herrera-Lormendez et al. 2023) and increase extreme precipitation. Additionally, a stronger north–south gradient over the North Atlantic leads to stronger westerlies (Kjellström et al. 2018), which was found to be strongest in EC-EARTH-driven and CNRM-CM5-driven models. This could be an indication of the strong CNRM-CM6-1 signals for the strong (thermo)dynamic signals for intensity changes in C, that we found here.

Our metric for extreme-rainfall intensity concerns the average excess rainfall on days of extreme rainfall. Another commonly used metric for rainfall intensity changes considers quantile changes (e.g., P99.9) between the future and historical period. This quantile-based rainfall intensity change is 11.9% in our study (see Table S1) which is comparable to our intensity change of 15.01%. However, as opposed to our intensity metric and as shown in Section S2, this quantile-based metric is a monotonically increasing function of extreme-rainfall likelihood changes $\Delta P_{\text{ext}}(x_t)$. In other words, positive (negative) changes in $\Delta P_{\text{ext}}(x_t)$ give rise to positive (negative) changes in the quantile-based intensity change. Thus, the sign of dynamical or thermodynamical contributions (per LWT, per season, etc.) for $\Delta P_{\text{ext}}(x_t)$ will be the same for the quantile-based intensity changes. Additionally, the decomposition Equation (3) is not well defined for quantile changes as the function $G(d)$ as introduced in Section S1 (necessarily a function of the day), cannot be identified.

Our conclusions on the contributions of dynamical and thermodynamical contributions to climate change remain qualitatively unchanged when using a lower threshold to define extreme rainfall. Figure S8 shows the relative changes in extreme-rainfall intensity and probability using the 95th quantile of daily rainfall instead of the 98.87th quantile to define extreme rainfall. For the 95th quantile the changes in extreme-rainfall intensity are

slightly higher but are statistically more robust, due to a large model agreement on the positive thermodynamical changes. As expected, upon lowering the threshold, the changes in extreme-rainfall probability are strongly reduced but their partitioning in dynamical and thermodynamical parts remains qualitatively similar.

5 | Conclusion

This work investigates the dynamical contributions underlying extreme daily precipitation events in Belgium, exploring the historical and projected future changes associated with LWTs using station observations and CMIP6 simulations.

Historical data indicate that wet cyclonic (C) weather types in fall and winter and westerly (W), and south-westerly (SW) in spring and summer are the primary drivers of extreme precipitation. Even though days with anticyclonic conditions occur most often, they rarely coincide with extreme rainfall. The GCM evaluation underscores significant differences in their ability to simulate weather types during all days and days with extreme precipitation, stressing the importance of targeted model selection. By applying the sPSS, 19 out of 24 models were retained for future projections, thereby excluding a model that was previously found to be one of the best models at representing the average circulation probability distribution over Belgium.

The end-of-the-century projections under the SSP3-7.0 scenario show a substantial increase in the intensity and likelihood of extreme-rainfall events. The dynamic contributions are generally small and insignificant with respect to the thermodynamic changes. The results underscore the critical role of thermodynamic processes in shaping future precipitation extremes. Therefore, this work provides an incentive for the use of methods such as the pseudo-global-warming approach (Schär et al. 1996) to probe the uncertainties related to the impact of climate change on extreme rainfall. Additionally, this work again highlights the necessity for targeted adaptation strategies to mitigate the growing risks associated with human-induced hydrological changes.

Further paths of interest include the investigation of the changes in extreme rainfall using projection data from regional climate models (RCMs) or convection-permitting models (Serras et al. 2024) rather than GCMs, the relation with temperature changes and the changes in rainfall extremes, the use of impact-tailored weather-type clustering methods (e.g., Serras et al. 2024) and, an extension of the framework in the context of attribution (Vautard et al. 2016) or subdaily rainfall extremes (Whitford et al. 2024). These, however, are considered beyond the scope of the current work.

Author Contributions

Jozefien Schoofs: writing – original draft, writing – review and editing, software, data curation, formal analysis, validation, visualization, investigation. **Kobe Vandelanotte:** methodology, writing – review and editing, software, data curation, visualization, conceptualization, supervision, investigation. **Hans Van de Vyver:** conceptualization, methodology, writing – review and editing, supervision, investigation. **Line Van Der Sichel:** software, data curation, formal analysis, validation, investigation. **Matthias Vandersteene:** software, data curation, formal analysis, validation, investigation. **Fien Serras:** writing – review and editing, methodology, software, data curation, visualization, investigation. **Nicole P. M. van Lipzig:** writing – review and editing, investigation. **Bert Van Schaeybroeck:** conceptualization, methodology, data curation, visualization, supervision, project administration, writing – review and editing, investigation.

Acknowledgements

We acknowledge Copernicus for the ERA5 reanalysis data. We also acknowledge the World Climate Research Programme, which, through its Working Group on Coupled Modelling, coordinated and promoted CMIP6. We thank the climate model groups for producing and making available their model output, the Earth System Grid Federation (ESGF) for archiving the data and providing access, and the multiple funding agencies that support CMIP6 and ESGF.

Funding

This study was supported by the Belgian Federal Science Policy Office (Grant No. B2/223/P1/CORDEXbeII).

Conflicts of Interest

The authors declare no conflicts of interest.

Data Availability Statement

The data that support the findings of this study are available in Climate Data Store at https://climate.copernicus.eu. These data were derived from the following resources available in the public domain: Copernicus Climate Change Service (C3S), https://cds.climate.copernicus.eu; ESGF, https://esgf-metagrid.cloud.dkrz.de; RMI opendata portal, https://opendata.meteo.be.

References

Athanase, M., A. Sánchez-Benítez, E. Monfort, T. Jung, and H. F. Goessling. 2024. "How Climate Change Intensified Storm Boris' Extreme Rainfall, Revealed by Near-Real-Time Storylines." *Communications Earth & Environment* 5: 676. https://doi.org/10.1038/s43247-024-01847-0.

Barry, R., and A. Perry. 1973. *Synoptic Climatology; Methods and Applications*. Methuen.

Belleflamme, A., X. Fettweis, C. Lang, and M. Erpicum. 2013. "Current and Future Atmospheric Circulation at 500 hPa Over Greenland Simulated by the CMIP3 and CMIP5 Global Models." *Climate Dynamics* 41: 2061–2080.

Brands, S. 2022. "A Circulation-Based Performance Atlas of the CMIP5 and 6 Models for Regional Climate Studies in the Northern Hemisphere Mid-To-High Latitudes." *Geoscientific Model Development* 15: 1375–1411. https://gmd.copernicus.org/articles/15/1375/2022/.

Brisson, E., M. Demuzere, B. Kwakernaak, and N. P. M. Van Lipzig. 2011. "Relations Between Atmospheric Circulation and Precipitation in Belgium." *Meteorology and Atmospheric Physics* 111: 27–39.

Brogli, R., S. L. Sorland, N. Kroner, and C. Schar. 2019. "Causes of Future Mediterranean Precipitation Decline Depend on the Season." *Environmental Research Letters* 14: 114017.

Cattiaux, J., H. Douville, A. Ribes, F. Chauvin, and C. Plante. 2013. "Towards a Better Understanding of Changes in Wintertime

Cold Extremes Over Europe: A Pilot Study With CNRM and IPSL Atmospheric Models." *Climate Dynamics* 40: 2433–2445.

Cotterill, D. F., J. O. Pope, and P. A. Stott. 2023. "Future Extension of the UK Summer and Its Impact on Autumn Precipitation." *Climate Dynamics* 60: 1801–1814. https://doi.org/10.1007/s00382-022-06403-0.

De Troch, R., C. Bertrand, M. Journée, et al. 2020. *Klimaatrapport 2020: Van Klimaatinformatie tot Klimaatdiensten*. Royal Meteorological Institute of Belgium. https://www.meteo.be/nl/klimaat/klimaatverandering-in-belgie/klimaatrapporten.

Demuzere, M., M. Werner, E. Roeckner, and N. Van Lipzig. 2009. "An Analysis of Present and Future ECHAM5 Pressure Fields Using a Classification of Circulation Patterns." *International Journal of Climatology* 29: 1796–1810.

Eyring, V., S. Bony, G. A. Meehl, et al. 2016. "Overview of the Coupled Model Intercomparison Project Phase 6 (CMIP6) Experimental Design and Organization." *Geoscientific Model Development* 9: 1937–1958. https://gmd.copernicus.org/articles/9/1937/2016/.

Faranda, D., G. Messori, A. Jezequel, M. Vrac, and P. Yiou. 2023. "Atmospheric Circulation Compounds Anthropogenic Warming and Impacts of Climate Extremes in Europe." *Proceedings of the National Academy of Sciences of the United States of America* 120: e2214525120.

Feng, T., X. Zhu, and W. Dong. 2023. "Historical Assessment and Future Projection of Extreme Precipitation in CMIP6 Models: Global and Continental." *International Journal of Climatology* 43: 4119–4135. https://rmets.onlinelibrary.wiley.com/doi/abs/10.1002/joc.8077.

Giorgi, F., F. Raffaele, and E. Coppola. 2019. "The Response of Precipitation Characteristics to Global Warming From Climate Projections." *Earth System Dynamics* 10: 73–89.

Grise, K. M., and S. M. Davis. 2020. "Hadley Cell Expansion in CMIP6 Models." *Atmospheric Chemistry and Physics* 20: 5249–5268. https://acp.copernicus.org/articles/20/5249/2020/.

Guo, H., S. He, M. Li, et al. 2022. "Future Changes of Drought Characteristics in Coupled Model Intercomparison Project Phase 6 Shared Socioeconomic Pathway Scenarios Over Central Asia." *International Journal of Climatology* 42: 3888–3908. https://rmets.onlinelibrary.wiley.com/doi/abs/10.1002/joc.7450.

Gutiérrez, J., R. Jones, G. Narisma, et al. 2021. "Atlas." In *Climate Change 2021: The Physical Science Basis. Contribution of Working Group I to the Sixth Assessment Report of the Intergovernmental Panel on Climate Change*, edited by V. Masson-Delmotte, P. Zhai, A. Pirani, et al., 1927–2058. Cambridge University Press. https://www.ipcc.ch/report/ar6/wg1/downloads/report/IPCC_AR6_WGI_Atlas.pdf.

Hansen, F., D. Belušić, and K. Wyser. 2024. "Relationship Between Circulation Types and Extreme Precipitation Over Scandinavia is Stable Under Climate Change." *Geophysical Research Letters* 51: e2024GL109704. https://agupubs.onlinelibrary.wiley.com/doi/abs/10.1029/2024GL109704.

Hellström, C. 2005. "Atmospheric Conditions During Extreme and Non-Extreme Precipitation Events in Sweden." *International Journal of Climatology* 25: 631–648. https://rmets.onlinelibrary.wiley.com/doi/abs/10.1002/joc.1119.

Herrera-Lormendez, P., A. John, H. Douville, and J. Matschullat. 2023. "Projected Changes in Synoptic Circulations Over Europe and Their Implications for Summer Precipitation: A CMIP6 Perspective." *International Journal of Climatology* 43: 3373–3390.

Hersbach, H., B. Bell, P. Berrisford, et al. 2020. "The ERA5 Global Reanalysis." *Quarterly Journal of the Royal Meteorological Society* 146: 1999–2049. https://rmets.onlinelibrary.wiley.com/doi/abs/10.1002/qj.3803.

Huth, R., C. Beck, A. Philipp, et al. 2008. "Classifications of Atmospheric Circulation Patterns: Recent Advances and Applications." *Annals of the New York Academy of Sciences* 1146: 105–152.

IPCC. 2021. *Climate Change 2021: The Physical Science Basis. Contribution of Working Group I to the Sixth Assessment Report of the Intergovernmental Panel on Climate Change*. Cambridge University Press. https://report.ipcc.ch/ar6/wg1/IPCC_AR6_WGI_FullReport.pdf.

IPCC. 2022. *Climate Change 2022: Impacts, Adaptation and Vulnerability. Contribution of Working Group II to the Sixth Assessment Report of the Intergovernmental Panel on Climate Change*. Cambridge University Press. https://report.ipcc.ch/ar6/wg2/IPCC_AR6_WGII_FullReport.pdf.

Jenkinson, A. F., and F. P. Collison. 1977. *An Initial Climatology of Gales Over the North Synoptic Climatology. Tech. Rep. Branch Memorandum 62*. UK Met. Office.

Journée, M., C. Delvaux, and C. Bertrand. 2015. "Precipitation Climate Maps of Belgium." *Advances in Science and Research* 12: 73–78. https://asr.copernicus.org/articles/12/73/2015/.

Kjellström, E., G. Nikulin, G. Strandberg, et al. 2018. "European Climate Change at Global Mean Temperature Increases of 1.5 and 2°C Above Pre-Industrial Conditions as Simulated by the Euro-CORDEX Regional Climate Models." *Earth System Dynamics* 9: 459–478. https://esd.copernicus.org/articles/9/459/2018/.

Kotz, M., S. Lange, L. Wenz, and A. Levermann. 2024. "Constraining the Pattern and Magnitude of Projected Extreme Precipitation Change in a Multimodel Ensemble." *Journal of Climate* 37: 97–111.

Kuettel, M., J. Luterbacher, and H. Wanner. 2011. "Multidecadal Changes in Winter Circulation-Climate Relationship in Europe: Frequency Variations, Within-Type Modifications, and Long-Term Trends." *Climate Dynamics* 36: 957–972.

Lamb, H., and G. B. M. Office. 1972. *British Isles Weather Types and a Register of the Daily Sequence of Circulation Patterns, 1861–1971. Geophysical Memoirs*. H.M. Stationery Office. https://books.google.be/books?id=RngmzwEACAAJ.

Lenggenhager, S., and O. Martius. 2019. "Atmospheric Blocks Modulate the Odds of Heavy Precipitation Events in Europe." *Climate Dynamics* 53: 4155–4171.

Li, C., F. Zwiers, X. Zhang, G. Li, Y. Sun, and M. Wehner. 2021. "Changes in Annual Extremes of Daily Temperature and Precipitation in CMIP6 Models." *Journal of Climate* 34: 3441–3460. https://journals.ametsoc.org/view/journals/clim/34/9/JCLI-D-19-1013.1.xml.

McSweeney, C., R. Jones, R. W. Lee, and D. Rowell. 2015. "Selecting CMIP5 GCMs for Downscaling Over Multiple Regions." *Climate Dynamics* 44: 3237–3260.

Mees, H., C. Suykens, J.-C. Beyers, B. Delvaux, K. Deketelaere, and A. Crabbé. 2015. "Analysing and Evaluating Flood Risk Governance in Belgium. Dealing With Flood Risks in an Urbanised and Institutionally Complex Country." Technical Report.

Neelin, J. D., C. Martinez-Villalobos, S. N. Stechmann, et al. 2022. "Precipitation Extremes and Water Vapor: Relationships in Current Climate and Implications for Climate Change." *Current Climate Change Reports* 8: 17–33.

O'Gorman, P. A. 2015. "Precipitation Extremes Under Climate Change." *Current Climate Change Reports* 1: 49–59.

O'Gorman, P. A., and T. Schneider. 2009. "The Physical Basis for Increases in Precipitation Extremes in Simulations of 21st-Century Climate Change." *Proceedings of the National Academy of Sciences of the United States of America* 106: 14773–14777.

Otero, N., J. Sillmann, and T. Butler. 2018. "Assessment of an Extended Version of the Jenkinson–Collison Classification on CMIP5 Models Over Europe." *Climate Dynamics* 50: 1559–1579. https://doi.org/10.1007/s00382-017-3705-y.

Pattison, I., and S. N. Lane. 2012. "The Relationship Between Lamb Weather Types and Long-Term Changes in Flood Frequency, River Eden, UK." *International Journal of Climatology* 32, no. 13: 1971–1989.

Perkins, S. E., A. J. Pitman, N. J. Holbrook, and J. McAneney. 2007. "Evaluation of the AR4 Climate Models' Simulated Daily Maximum Temperature, Minimum Temperature, and Precipitation Over Australia Using Probability Density Functions." *Journal of Climate* 20: 4356–4376.

Perks, R. J., D. Bernie, J. Lowe, and R. Neal. 2023. "The Influence of Future Weather Pattern Changes and Projected Sea-Level Rise on Coastal Flood Impacts Around the UK." *Climatic Change* 176: 25. https://doi.org/10.1007/s10584-023-03496-2.

Pfahl, S. 2014. "Characterising the Relationship Between Weather Extremes in Europe and Synoptic Circulation Features." *Natural Hazards and Earth System Sciences* 14: 1461–1475. https://nhess.copernicus.org/articles/14/1461/2014/.

Pfahl, S., P. A. O'Gorman, and E. M. Fischer. 2017. "Understanding the Regional Pattern of Projected Future Changes in Extreme Precipitation." *Nature Climate Change* 7: 423–427.

Planchon, O., H. Quénol, N. Dupont, and S. Corgne. 2009. "Application of the Hess-Brezowsky Classification to the Identification of Weather Patterns Causing Heavy Winter Rainfall in Brittany (France)." *Natural Hazards and Earth System Sciences* 9: 1161–1173.

Poelmans, L., A. Van Rompaey, and O. Batelaan. 2010. "Coupling Urban Expansion Models and Hydrological Models: How Important Are Spatial Patterns?" *Land Use Policy* 27: 965–975. https://www.sciencedirect.com/science/article/pii/S0264837709002130.

Pope, J. O., K. Brown, F. Fung, et al. 2022. "Investigation of Future Climate Change Over the British Isles Using Weather Patterns." *Climate Dynamics* 58: 2405–2419.

Prein, A. F., P. A. Mooney, and J. M. Done. 2023. "The Multi-Scale Interactions of Atmospheric Phenomenon in Mean and Extreme Precipitation." *Earth's Future* 11: e2023EF003534. https://agupubs.onlinelibrary.wiley.com/doi/abs/10.1029/2023EF003534.

Richardson, D., H. J. Fowler, C. G. Kilsby, R. Neal, and R. Dankers. 2020. "Improving Sub-Seasonal Forecast Skill of Meteorological Drought: A Weather Pattern Approach." *Natural Hazards and Earth System Sciences* 20: 107–124. https://nhess.copernicus.org/articles/20/107/2020/.

Richardson, D., H. J. Fowler, C. G. Kilsby, and R. Neal. 2018. "A New Precipitation and Drought Climatology Based on Weather Patterns." *International Journal of Climatology* 38: 630–648. https://rmets.onlinelibrary.wiley.com/doi/abs/10.1002/joc.5199.

Richardson, D., R. Neal, R. Dankers, et al. 2020. "Linking Weather Patterns to Regional Extreme Precipitation for Highlighting Potential Flood Events in Medium- to Long-Range Forecasts." *Meteorological Applications* 27: e1931. https://rmets.onlinelibrary.wiley.com/doi/abs/10.1002/met.1931.

RMI Atlas. 2024. "Klimaatatlas." Accessed October 31, 2024. https://www.meteo.be/nl/klimaat/klimaat-van-belgie/klimaatatlas/klimaatkaarten/neerslag/neerslaghoeveelheid/jaarlijks.

Schär, C., C. Frei, D. Lüthi, and H. C. Davies. 1996. "Surrogate Climate-Change Scenarios for Regional Climate Models." *Geophysical Research Letters* 23: 669–672.

Schiemann, R., and C. Frei. 2010. "How to Quantify the Resolution of Surface Climate by Circulation Types: An Example for Alpine Precipitation." *Physics and Chemistry of the Earth* 35: 403–410.

Serras, F., K. Vandelanotte, R. Borgers, et al. 2024. "Optimizing Climate Model Selection in Regional Studies Using an Adaptive Weather Type Based Framework: A Case Study for Extreme Heat in Belgium." *Climate Dynamics* 62: 9927–9949. https://doi.org/10.1007/s00382-024-07432-7.

Shepherd, T. G. 2014. "Atmospheric Circulation as a Source of Uncertainty in Climate Change Projections." *Nature Geoscience* 7: 703–708.

Souverijns, N., W. Thiery, M. Demuzere, and N. P. M. V. Lipzig. 2016. "Drivers of Future Changes in East African Precipitation." *Environmental Research Letters* 11: 114011.

Tabari, H., K. Madani, and P. Willems. 2020. "The Contribution of Anthropogenic Influence to More Anomalous Extreme Precipitation in Europe." *Environmental Research Letters* 15: 104077. https://doi.org/10.1088/1748-9326/abb268.

Termonia, P., B. Van Schaeybroeck, L. De Cruz, et al. 2018. "The CORDEX.be Initiative as a Foundation for Climate Services in Belgium." *Climate Services* 11: 49–61. https://www.sciencedirect.com/science/article/pii/S2405880717300195.

Thackeray, C. W., A. Hall, J. Norris, and D. Chen. 2022. "Constraining the Increased Frequency of Global Precipitation Extremes Under Warming." *Nature Climate Change* 12: 441–448.

Tradowsky, J. S., S. Y. Philip, F. Kreienkamp, et al. 2023. "Attribution of the Heavy Rainfall Events Leading to Severe Flooding in Western Europe During July 2021." *Climatic Change* 176: 90. https://doi.org/10.1007/s10584-023-03502-7.

Tramblay, Y., L. Neppel, J. Carreau, and K. Najib. 2013. "Non-Stationary Frequency Analysis of Heavy Rainfall Events in Southern France." *Hydrological Sciences Journal* 58: 280–294.

Trigo, R. M., and C. C. DaCamara. 2000. "Circulation Weather Types and Their Influence on the Precipitation Regime in Portugal." *International Journal of Climatology* 20: 1559–1581. https://rmets.onlinelibrary.wiley.com/doi/abs/10.1002/1097-0088%2820001115%2920%3A13%3C1559%3A%3AAID-JOC555%3E3.0.CO%3B2-5.

Van de Vyver, H. 2012. "Spatial Regression Models for Extreme Precipitation in Belgium." *Water Resources Research* 48: W09549. https://agupubs.onlinelibrary.wiley.com/doi/abs/10.1029/2011WR011707.

Vanden Broucke, S., H. Wouters, M. Demuzere, and N. van Lipzig. 2019. "The Influence of Convection-Permitting Regional Climate Modeling on Future Projections of Extreme Precipitation: Dependency on Topography and Timescale." *Climate Dynamics* 52: 5303–5324.

Vautard, R., J. Cattiaux, T. Happé, et al. 2023. "Heat Extremes in Western Europe Increasing Faster Than Simulated due to Atmospheric Circulation Trends." *Nature Communications* 14: 6803.

Vautard, R., P. Yiou, F. Otto, et al. 2016. "Attribution of Human-Induced Dynamical and Thermodynamical Contributions in Extreme Weather Events." *Environmental Research Letters* 11: 114009.

VMM. 2023. "Neerslagextremen (1892–2022/2023)." Accessed October 21, 2024. https://www.vmm.be/klimaat/neerslagextremen/.

Whitford, A. C., S. Blenkinsop, and H. J. Fowler. 2024. "Atmospheric Patterns Associated With Summer Sub-Daily Rainfall Extremes in Western Europe." *Climate Dynamics* 62: 10131–10152.

World Weather Attribution. 2024. "Extreme Downpours Increasing in Southern Spain as Fossil Fuel Emissions Heat the Climate." Accessed November 12, 2024. https://www.worldweatherattribution.org/extreme-downpours-increasing-in-southern-spain-as-fossil-fuel-emissions-heat-the-climate/.

Wyard, C., C. Scholzen, X. Fettweis, J. Van Campenhout, and L. François. 2017. "Decrease in Climatic Conditions Favouring Floods in the South-East of Belgium Over 1959–2010 Using the Regional Climate Model MAR." *International Journal of Climatology* 37: 2782–2796. https://rmets.onlinelibrary.wiley.com/doi/abs/10.1002/joc.4879.

Zappa, G., L. C. Shaffrey, K. I. Hodges, P. G. Sansom, and D. B. Stephenson. 2013. "A Multimodel Assessment of Future Projections of North Atlantic and European Extratropical Cyclones in the CMIP5 Climate Models." *Journal of Climate* 26: 5846–5862.

Supporting Information

Additional supporting information can be found online in the Supporting Information section. **Figure S1:** Same as Figure 1 but for the different LWTs over the study domain. **Figure S2:** Barplots representing the historical weather-type probability. **Figure S3:** Same as Figure 3 but ranking models based on the Perkins Skill Score (PSS) instead of squared Perkins Skill Score (sPSS). **Figure S4:** Same as Figure 3 but using the 95th quantile of daily rainfall as threshold for extreme rainfall instead of the 98.87th quantile. **Figure S5:** Same as Figure 3 but PSS instead of sPSS, and, using the 95th quantile of daily rainfall as threshold for extreme rainfall instead of the 98.87th quantile. **Figure S6:** The PSS and sPSS associated with the climatological LWT probability (Q_{clim}) against the corresponding score associated with the LWT probability during extreme-rainfall days (Q_{ext}). **Figure S7:** Same as Figure 4 but showing absolute instead of relative changes. **Figure S8:** Same as Figure 4 but using the 95th quantile of daily rainfall as threshold for extreme rainfall instead of the 98.87th quantile. **Figure S9:** Same as Figure 5 but showing absolute instead of relative changes. **Figure S10:** Barplots showing the contributing terms to Equation (2) per weather type. **Figure S11:** The PSS and sPSS score associated with the LWT probability Q_{cond} and the one associated with the climatological LWT probability (Q_{clim}) versus the PSS and sPSS score associated with Q_{ext}. **Figure S12:** Model biases in extreme rainfall intensity and probability against the model rank based on sPSS. **Table S1:** Overview of the CMIP6 models used in this project. **Section S1:** General analytical derivation of Equations (1) and (2), that is the decomposition into thermodynamic and dynamic contributions. **Section S2:** This section addresses the mathematical relation between the extreme-rainfall changes and quantile-based intensity changes.